GW approximations and vertex corrections on the Keldysh time-loop contour: Application for model systems at equilibrium

H. Ness,[1,2,*] L. K. Dash,[1,2] M. Stankovski,[3,2] and R. W. Godby[1,2]
[1]*Department of Physics, University of York, Heslington, York YO10 5DD, United Kingdom*
[2]*European Theoretical Spectroscopy Facility (ETSF)*
[3]*IMCN-NAPS, Université Catholique de Louvain, Place Croix du Sud 1 bte 3, BE-1348 Louvain-la-Neuve, Belgium*
(Received 6 June 2011; revised manuscript received 7 November 2011; published 21 November 2011)

We study the effects of self-consistency and vertex corrections on different GW-based approximations for model systems of interacting electrons. For dealing with the most general case, we use the Keldysh time-loop contour formalism to evaluate the single-particle Green's functions. We provide the formal extension of Hedin's GW equations for the Green's function in the Keldysh formalism. We show an application of our formalism to the plasmon model of a core electron within the plasmon-pole approximation. We study in detail the effects of the diagrammatic perturbation expansion of the core-electron/plasmon coupling on the spectral functions in the so-called S model. The S model provides an exact solution at equilibrium for comparison with the diagrammatic expansion of the interaction. We show that self-consistency is essential in GW-based calculations to obtain the full spectral information. The second-order exchange diagram (i.e., a vertex correction) is also crucial to obtain the good spectral description of the plasmon satellites. We corroborate these results by considering conventional equilibrium GW-based calculations for the pure jellium model. We find that with no second-order vertex correction, one cannot obtain the full set of plasmon side-band resonances. We also discuss in detail the formal expression of the Dyson equations obtained for the time-ordered Green's function at zero and finite temperature from the Keldysh formalism and from conventional equilibrium many-body perturbation theory.

DOI: 10.1103/PhysRevB.84.195114 PACS number(s): 71.10.Ca, 71.10.−w, 71.15.−m, 71.45.Gm

I. INTRODUCTION

Equilibrium, zero- and finite-temperature Green's functions techniques based on many-body perturbation theory (MBPT) are widely used in electronic-structure and total energy calculations.[1] Hedin's formulation[2,3] for the electronic Green's function closes the many-body hierarchy by expanding the electron self-energy of the one-particle Green's function in terms of the screened Coulomb interaction in the presence of vertex corrections.

Without these vertex corrections, one obtains the conventional GW equations.[3–8] The GW method is an approximate treatment of the propagation of electrons: it can be seen as if electrons interact with themselves via a Coulomb interaction that is screened by virtual electron-hole pairs. In bulk semiconductors, the GW approximation is known to lead to surprisingly accurate band gaps,[4,6,7,9] while for finite-size systems and molecules the method provides qualitatively correct values of ionization energies and electron affinities.[10] It also provides a convenient starting point for many useful approximations and applications to photoemission spectroscopy[8] and optical absorption in metals or semiconductors as well as in finite-size molecular systems.[6,10–13] Most practical GW calculations today are performed in a perturbative manner using equilibrium MBPT.

However, if we want to consider a system driven out of equilibrium by an external "force,' such as, for example, a molecular wire coupled to electrodes sustaining an electronic current flow or any system driven by an external electromagnetic field (time-dependent or not), we need to extend the equations for the dynamics of the quantum many-body interacting system (Hedin's equations or their simplified GW form) to nonequilibrium conditions.

For this, the nonequilibrium Green's function (NEGF) technique[14–17] has been widely used to calculate electronic transport properties of mesoscopic[18] and nanoscale[19–24] systems, plasmas, quantum transport in semiconductors[18] and high-energy processes in nuclear physics.[25] Also known as the closed time-path formalism,[26,27] the NEGF formalism depends on an "artificial" time parameter that runs on a mathematically convenient time-loop contour (plus eventually an imaginary time for taking into account the initial correlation and statistical boundary conditions). It is a formal procedure that only has a direct physical meaning when one projects back the time parameters of the time-loop contour onto real times. It was introduced because it allows one to obtain self-consistent Dyson-like equations for the Keldysh Green's function using Schwinger's functional derivative technique. Transforming the Dyson equation to real time by varying the Keldysh time parameter over the time-loop contour results in a set of self-consistent equations for the different nonequilibrium Green's functions (advanced/retarded or lesser/greater). The NEGF technique is general and can treat nonequilibrium as well as equilibrium conditions, and the zero- and finite-temperature limits, within a single framework.

The NEGF technique has been applied to the study of different levels of self-consistency in the GW approach for atoms, molecules, and semiconductors in Refs. 28–34. However, these works did not include the effects of simultaneous self-consistency and vertex corrections. Other levels of approximation for electron-electron interactions have also been considered in finite-size nanoclusters by using the Kadanoff-Baym flavor of NEGF.[35,36]

In this paper, we want to study these effects (self-consistency and vertex corrections) and use the most general formalism to deal with the full equivalent to Hedin's GW

equations. We believe that the Keldysh formalism, even applied to equilibrium conditions, can be more useful than the conventional approaches since it is by nature a more general approach.

We extend Hedin's equations to the Keldysh time-loop contour, and derive the equations for the one-particle Green's function G, self-energy Σ, screened Coulomb interaction W, and for the (three-point) vertex functions Γ. Note that a nonequilibrium approach to Hedin's GW equations has been provided in Ref. 37 where an alternative distinct approach based on the Liouvillian superoperator formalism is used. However, working in a Louivillian vector space is much less convenient and much more computationaly demanding for practical applications than working within a Hilbert space as in the formalism we develop below.

We then apply our formalism to the calculation of the spectral function of a particular model of a homogeneous electron gas: the plasmon model for a core electron.[3,38,39] We choose this model as it can be solved exactly at equilibrium, and thus we are able to compare the different approximations introduced in the calculations (self-consistency versus one-shot calculations and/or vertex corrections) and check their validity for different limiting cases (the high- and low-electronic-density regimes). We also compare the outcome of these calculations with conventional GW calculations for the jellium model. We examine if the effects on the spectral functions rendered by self-consistency iterations and the inclusion of vertex corrections that we find for the plasmon model with a core electron also hold for the jellium model.

To our knowledge, the only available exact results are for equilibrium conditions, and thus we benchmark our formalism against exact results at equilibrium before extending the discussion to nonequilibrium conditions.

The paper is organized as follows. In Sec. II, we recall the expressions of Hedin's GW equations and briefly review the performance of conventional GW calculations. The extension of Hedin's equations to the Keldysh time-loop contour is provided in Sec. III. We also show that we recover the conventional nonequilibrium GW formalism developed and used by others[28,31–34] when ignoring the vertex corrections in Appendix C. The lowest-order expansion, in terms of the interaction for the screened Coulomb interaction W and for the vertex functions Γ, is given in Appendix C. In Appendix D, we also provide a rigorous mathematical proof of the difference between equilibrium time-ordered Green's functions in the zero- and finite-temperature limits that were discussed less rigorously in Chap. IV.17 of Ref. 3.

In Sec. IV, we apply our formalism to the calculation of the spectral function of a model system and core electron coupled to a plasmon mode.[3,38,39] The exact solution of this model at equilibrium permits us to examine the effects of self-consistency and vertex corrections on the spectral density. We also examine these effects for another model of an electron gas, the jellium model, by using conventional GW calculations (see Sec. IV E). We show a general trend: second-order diagrams for the interactions (i.e., vertex corrections) are necessary to obtain the full series of plasmon side-band peaks. Finally, we conclude our work in Sec. V.

II. HEDIN'S GW EQUATIONS

Hedin's GW equations[2,3] were originally derived for the time-ordered single-particle Green's function G at equilibrium, defined by

$$G(12) = -\mathrm{i}\langle \mathcal{T}\Psi(1)\Psi^\dagger(2)\rangle\ . \tag{1}$$

They are expressed as follows:[2,3]

$$G(12) = G_0(12) + \int \mathrm{d}(34)\ G_0(13)\ \Sigma(34)\ G(42), \tag{2a}$$

$$\Sigma(12) = \mathrm{i}\int \mathrm{d}(34)\ G(13)\ \Gamma(32;4)\ W(41), \tag{2b}$$

$$W(12) = v(12) + \int \mathrm{d}(34)\ v(13)\ \tilde{P}(34)\ W(42), \tag{2c}$$

$$\tilde{P}(12) = -\mathrm{i}\int \mathrm{d}(34)\ G(13)\ G(41)\ \Gamma(34;2), \tag{2d}$$

$$\Gamma(12;3) = \delta(12)\delta(13) + \int \mathrm{d}(4567)\ \frac{\delta\Sigma(12)}{\delta G(45)} \times G(46)\ G(75)\ \Gamma(67;3), \tag{2e}$$

with the usual notation for the space-time coordinates; any integer i represents a point in space-time $\underline{i} = \mathbf{x}_i = (\mathbf{r}_i, t_i)$, and for the electron single-particle Green's function G, the corresponding self-energy Σ, the screened Coulomb interaction W, the irreducible polarizability $\tilde{P}$ (sometimes also called polarization), and the vertex function Γ.

Up to now, most practical GW calculations are performed not fully self-consistently, using a single iteration of the GW equations, called one-shot GW or G_0W_0. When a single iteration is performed, the initial approximation must be good, so typically G_0 is constructed from the orbitals of any current ground-state method, which correctly predicts the basic physics of the system.

The application of G_0W_0 corrections to spectral properties and band gaps as calculated in the local density approximation (LDA) and generalized gradient approximation (GGA) in density functional theory (DFT) is a long-standing success story,[40] at least for many s-p bonded systems. However, total energies calculated from the Galitskii-Migdal formula at the G_0W_0 level are generally worse than those given by other ground-state methods. The initial close agreements with measured band gaps were later shown to be partly due to technical approximations used along the way. Several studies have shown that LDA+G_0W_0 systematically underestimates band gaps when solved in state-of-the-art all-electron schemes with full explicit treatment of frequency integrals (gaps are underestimated by about 1–10% for s-p bonded systems and about 20–50% for systems with d electrons, like rare-earth oxides, sulfides, and nitrides).[41,42] The remaining discrepancy has prompted the search for more accurate but still tractable methods.

In general, attempts at fully self-consistent GW have shown that spectral properties worsen as compared with G_0W_0, while total energies improve. GW band gaps were first shown to be larger than expected in a quasi one-dimensional Si wire model by de Groot *et al.*[43] Von Barth and Holm showed that in jellium for a self-consistent update only of the Green's function (a GW_0 approach), a displacement of weight from quasiparticle peaks into the incoherent background occurs.[44] Also, the occupied bandwidth broadens rather than narrows, as expected from experiments on simple metals. At the same time, E. L. Shirley showed that the bandwidth of jellium broadens further with full self-consistency, while the bandwidth narrows again once vertex corrections are taken into account.[45] The effects of nonlocality in vertex corrections were also addressed in Ref. 46.

Later studies have shown that GW total energies for jellium are very accurate,[47–49] as expected from a conserving approximation in the Baym-Kadanoff sense.[50] This holds true even for low-dimensional atomic and molecular systems, and ionization potentials as calculated by the extended Koopman's theorem also tend to be accurate.[29,34,51] Full GW calculations were performed by Kutepov *et al.* for simple metals and semiconductors, They showed *inter alia* that the calculated equilibrium lattice parameters were all very close to the experimental ones.[52]

In view of improving the starting point, quasiparticle self-consistent GW has emerged as a good compromise between self-consistency and a practical path to good spectral properties.[53] It has been shown that vertex corrections further improve the correspondence between theory and experiment,[54] but consistently accurate results still remain elusive for systems with localized states, defects, and band offsets.[55–57]

In particular relevance to the present paper, no existing implementation of GW seems to describe the full spectrum of plasmon satellites in metals.

III. EXTENSION OF HEDIN's GW EQUATIONS TO THE KELDYSH TIME-LOOP CONTOUR

We now consider the generalization of the single-particle Green's function on the time-loop contour [the so-called Keldysh contour C_K with two branches, branch $(+)$ for forward time evolution and branch $(-)$ for backward time evolution]:

$$G(12) = -\mathrm{i}\langle \mathcal{T}_{C_K} \Psi(1)\Psi^\dagger(2)\rangle\ . \tag{3}$$

For the moment, we do not specify the nature of the "external force" that drives the system out of equilibrium. We consider the generalized Green's function on the Keldysh time-loop contour and hence end up with four different Keldysh components for the Green's functions: $G^{++}, G^{+-}, G^{-+}, G^{--}$, defined according to the way the two real-time arguments (t_1,t_2) are positioned on the time-loop contour C_K. The initial correlations (i.e., the initial boundary conditions) are assumed to be dealt with in an appropriate way.[15,17,22]

To derive the NE-GW equations, we proceed as follows: in each integral $\int d(1)$, the time is integrated over the time-loop contour C_K: $\int_{C_K} d\tau_1$, and then decomposed onto the two real-time branches: $\int_{C_K} d\tau_1 \equiv \int_{(+)} dt_1^+ + \int_{(-)} dt_1^- = \int dt_1^+ - \int dt_1^-$. We then calculate the different components $X^{\eta_1\eta_2}$ (with $\eta_{1,2} = \pm$) for the Green's function, self-energy, screened Coulomb interaction W, polarizability P, and vertex function Γ. Where possible, we reexpress these in a more convenient way by using the relations between the different Green's functions and self-energies on the time-loop contour (see Appendix A).

There are actually three kinds of equation in Hedin's GW Eqs. (2a)–(2e). First, there is a set of Dyson-like equations for the electron Green's function G and for the boson Green's function W, i.e., the screened Coulomb interaction. In these two equations, the vertex function Γ does not appear explicitly. Next, there is another set of equations for the electron self-energy Σ and for the polarizability (the boson self-energy) $\tilde{P}$. In these equations, the vertex function appears explicitly. Finally, there is the equation for the vertex function itself, Γ. The vertex function can be expanded as a series $\Gamma(12;3) = \sum_n \Gamma_{(n)}(12;3)$, where the index n represents the number of times the screened Coulomb interaction W appears explicitly in the series expansion. Each occurrence of the screened Coulomb interaction W in the vertex function Γ is generated by the functional derivative $\delta\Sigma/\delta G$.

Finally, one should note that the equilibrium properties of the system are, in principle, recovered from the extension of Hedin's GW equations to the Keldysh time-loop contour when the external driving force is omitted and the whole system is at thermodynamical equilibrium.

A. The electron Green's function and the self-energy

Following the prescriptions given above, we calculate the components G^{++}, G^{+-}, and G^{-+} from the extension of Eq. (2) on the time-loop contour, and we find the Dyson-like equation for $G^{r,a}$:

$$G^{r,a}(12) = G_0^{r,a}(12) + \int d(34)\ G_0^{r,a}(13)\Sigma^{r,a}(34)G^{r,a}(42), \tag{4}$$

which has the same functional form as in Eq. (2).

We also obtain the following quantum kinetic equation (QKE) for $G^{\lessgtr}$:

$$\begin{aligned} G^{\lessgtr}(12) = &\int d(3456)[\delta(14) + G^r(13)\Sigma^r(34)] \\ &\times G_0^{\lessgtr}(45)[\delta(52) + \Sigma^a(56)G^a(62)] \\ &+ \int d(34)\ G^r(13)\ \Sigma^{\lessgtr}(34)\ G^a(42). \end{aligned} \tag{5}$$

B. The screened Coulomb potential

By looking at Eq. (2c), one can see that W has the same functional form as the electron Green's function G. The screened Coulomb interaction W is a bosonic Green's function with an associated bosonic self-energy, the polarizability $\tilde{P}$. With the formal equivalence $(G,\Sigma) \leftrightarrow (W,\tilde{P})$, one can expect to obtain a Dyson-like equation for the advanced and retarded screened Coulomb interactions and a quantum kinetic equation for $W^{\lessgtr}$ as equivalently obtained for the electron Green's function.

This is indeed what we find: $W^{r,a}$ follows the usual Dyson-like equation as

$$W^{r,a}(12) = v(12) + \int d(34)\ v(13)\ \tilde{P}^{r,a}(34)\ W^{r,a}(42) \tag{6}$$

or in a more compact notation,

$$\begin{aligned} W^{r,a} &= v + v\tilde{P}^{r,a}W^{r,a} = v + W^{r,a}\tilde{P}^{r,a}v \\ &= v[1 - \tilde{P}^{r,a}v]^{-1} = [1 - v\tilde{P}^{r,a}]^{-1}v, \end{aligned} \tag{7}$$

where any product XY implies a space-time integration $[XY](12) = \int d(3)X(13)Y(32)$.

Since the bare Coulomb potential $v(12)$ is instantaneous, it corresponds to an interaction local in time and therefore its extension to the Keldysh contour has no v^{+-} or v^{-+} components. Hence, we obtain the following quantum kinetic equations for $W^{\lessgtr}$:

$$W^{\lessgtr}(12) = \int \mathrm{d}(34)\; W^r(13)\; \tilde{P}^{\lessgtr}(34)\; W^a(42). \tag{8}$$

C. The vertex function $\Gamma(12;3)$ on the contour C_K

The derivation of $\Gamma(12;3)$ on C_K does not create any formal difficulties. However, since $\Gamma(12;3)$ is a three-point function, it is not possible to recover a Dyson-like or a quantum-kinetic-like equation for Γ.

For any Keldysh components of the vertex function $\Gamma^{\eta_3\eta_2\eta_4}(32;4)$, we can formally write the different components of the self-energy on the Keldysh contour as follows:

$$\Sigma^{\eta_1\eta_2}(12) = \mathrm{i} \sum_{\eta_3\eta_4} \eta_3\eta_4 \int \mathrm{d}(34) \times G^{\eta_1\eta_3}(13)\; \Gamma^{\eta_3\eta_2\eta_4}(32;4)\; W^{\eta_4\eta_1}(41), \tag{9}$$

and likewise for the polarizability,

$$\tilde{P}^{\eta_1\eta_2}(12) = -\mathrm{i} \sum_{\eta_3\eta_4} \eta_3\eta_4 \int \mathrm{d}(34) G^{\eta_1\eta_3}(13) \times G^{\eta_4\eta_1}(41)\; \Gamma^{\eta_3\eta_4\eta_2}(34;2). \tag{10}$$

Now we need to close the above equations, i.e., to find an equation for the different components $\Gamma^{\eta_1\eta_2\eta_3}(12;3)$ of the vertex function. By considering the equivalent of Eq. (2e) on the Keldysh contour, we obtain

$$\Gamma^{\eta_1\eta_2\eta_3}(12;3) = \delta^{\eta_1\eta_2}(12)\delta^{\eta_1\eta_3}(13) + \sum_{\eta_4\ldots\eta_7} \eta_4\eta_5\eta_6\eta_7 \times \int \mathrm{d}(4567)\; \frac{\delta\Sigma^{\eta_1\eta_2}(12)}{\delta G^{\eta_4\eta_5}(45)} G^{\eta_4\eta_6}(46) \times G^{\eta_7\eta_5}(75)\Gamma^{\eta_6\eta_7\eta_3}(67;3). \tag{11}$$

In Appendix C, we consider the series expansion of the vertex function $\Gamma(12;3) = \sum_n \Gamma_{(n)}(12;3)$, where the index n represents the number of times the screened Coulomb interaction W appears explicitly in the series expansion, and we provide explicit results for the electron self-energy Σ and polarizability P for the lowest-order terms $\Gamma_{(0)}(12;3)$ and $\Gamma_{(1)}(12;3)$.

IV. APPLICATION TO MODELS RELATED TO THE HOMOGENEOUS ELECTRON GAS

Now we want to test our extended formalism of Hedin's GW equation onto the Keldysh time-loop contour and the corresponding series expansion of the vertex functions. The importance of self-consistency and vertex corrections was discussed in Sec. II. Self-consistency and vertex corrections apply in both equilibrium and nonequilibrium systems and therefore are more conveniently addressed in as simple a model system as possible.

Calculations could be performed for several model systems, but would not lead to any pertinent conclusions if they could not be compared to exact results. To our knowledge, exact results for interacting electron systems are few and not as widespread as numerical (highly accurate) calculations even for models of interacting electron systems. One of the available exactly-solvable models has been used in the context of x-ray spectroscopy of metals, and leads to tractable analytical expressions for the electron Green's function: the plasmon model for the core electron.[38]

In the next section, we consider this exactly-solvable model and compare the exact results with those obtained from our GW formalism, at zero and finite temperatures and with or without lowest-order vertex corrections. We note here that the exact solution is obtained for a model of a homogeneous electron gas *at equilibrium*. Dealing with an interacting system at equilibrium does not cause any problem within our formalism, since the equilibrium condition is just a special case of our more general formalism for nonequilibrium conditions (see appendix D for a full discussion about the equilibrium limit of the Keldysh formalism at zero and finite temperatures).

A. Effective Hamiltonian for the plasmon model of a core electron

The properties of a homogeneous 3D electron gas can be well described within the plasmon model. The plasmon model is defined from Hedin's equations Eqs. (2a)–(2e) together with the so-called plasmon-pole parametrization. In reciprocal space, the screened Coulomb potential can be written as $W(\omega,q) = v_q\; \epsilon^{-1}(\omega,q)$, where v_q is the Fourier component q of the Coulomb potential. The dielectric function $\epsilon^{-1}(\omega,q)$ is then obtained from the plasmon-pole approximation $\epsilon^{-1}(\omega,q) = 1 + \omega_p^2/(\omega^2 - \omega_q^2)$, where ω_p is the bulk plasmon energy, related to the electron density n as usual, $\omega_p^2 = (4\pi n e^2/m)$, and the plasmon dispersion ω_q remains to be defined.

Within this model, the dynamic part of the Coulomb potential $W(\omega,q) - v_q$ can be reexpressed as

$$v_2 = v_q[\epsilon^{-1}(\omega,q) - 1] = \frac{v_q\omega_p^2}{2\omega_q}\; \frac{2\omega_q}{\omega^2 - \omega_q^2} = \gamma_q^2\; B(\omega,q), \tag{12}$$

which involves a coupling constant γ_q and the bosonic propagator $B(\omega,q)$ of the plasmon modes.

Following Refs. 3, 38 and 39, we consider the following Hamiltonian for the plasmon model of a core electron:

$$H_{\text{eff}} = \varepsilon_c c^\dagger c + \sum_q \omega_q b_q^\dagger b_q + \sum_q \gamma_q c^\dagger c(b_q + b_{-q}^\dagger). \tag{13}$$

For this model of the core-electron case there exists a precise and well defined relation between the solution defined by a plasmon model for an electron gas and the solution defined by the corresponding effective Hamiltonian H_{eff}.[39] Finally, we consider the $q \to 0$ limit of static random-phase approximation[3] for the plasmon dispersion:

$$\omega_q = \omega_p \left[\frac{q^4}{(\omega_p^0)^2} + \frac{16}{3} \frac{q^2}{(\omega_p^0)^2} + 1 \right]^{1/2}, \tag{14}$$

with $\omega_p^0 = \omega_p/\varepsilon_F = 4(\frac{\alpha r_S}{3\pi})^{1/2}$, $\alpha = (\frac{4}{9\pi})^{1/3}$, and r_S defines the electron density $n = (\frac{4\pi}{3} r_S^3)^{-1}$.

B. The S model

A particularly simple model of a core electron, known as the S model,[39] is obtained by further replacing ω_q^{-1} by a step function $\omega_q^{-1} \to \omega_p^{-1}\theta(q_c - q)$, where the cutoff parameter q_c is determined by

$$q_c = \int_0^{q_c} dq = \int_0^{\infty} \frac{\omega_p^2}{\omega_q^2}\, dq. \tag{15}$$

From this definition of q_c, it follows that the energy-shift parameter

$$D = \sum_q \frac{\gamma_q^2}{\omega_q} = \frac{1}{2}\sum_q v_q \frac{\omega_p^2}{\omega_q^2}, \tag{16}$$

is the same as for the corresponding plasmon model.

The solution of the S model can be mapped onto a simpler Hamiltonian, giving rise to the same spectral information:

$$H_{\text{eff}} = \varepsilon_c c^\dagger c + \omega_p b^\dagger b + \gamma_0 c^\dagger c (b + b^\dagger), \tag{17}$$

with $\gamma_0^2 = D\omega_p$. An analytical expression for the relaxation energy D is found from the chosen dispersion relation of the plasmon frequency ω_q. We then find that the corresponding relaxation energy is given by

$$D = \sum_q \frac{\gamma_q^2}{\omega_q} = \frac{1}{2}\int \frac{d^3q}{(2\pi)^3} v_q \frac{\omega_p^2}{\omega_q^2} = \frac{1}{2\sqrt{2}} \frac{\omega_p^0}{\left(\omega_p^0 + \frac{8}{3}\right)^{1/2}}. \tag{18}$$

This result is very similar to the relaxation energy found by Minnhagen[39] when one replaces the prefactor 16/3 in the dispersion relation ω_q by 4/3 and when one uses the trigonometric relations $\sin(a/2) = \sqrt{(1-\cos a)/2}$ and $\cos[\tan^{-1}(u)] = 1/\sqrt{(1+u^2)}$.

The other advantage of dealing with the S model is that it has an exact solution[38,39,58] that can be compared with approximate calculations performed with Hedin's GW equation for different levels of expansion of the self-energy and/or vertex function. The exact solution of the S model at zero temperature provides us with an analytical expression for the retarded Green's function, given by

$$G^r(\omega) = \sum_{n=0}^{\infty} e^{-\gamma^2} \frac{\gamma^{2n}}{n!} \frac{1}{\omega - \tilde{\varepsilon}_c + n\omega_p + i\eta}, \tag{19}$$

with $\gamma^2 = (\gamma_0/\omega_p)^2 = D/\omega_p$ and the renormalized core level $\tilde{\varepsilon}_c = \varepsilon_c + D = \varepsilon_c + \gamma^2\omega_p$. The finite-temperatures solution is obtained from the prescription given in Ref. 58.

C. Feynman diagrams for the self-energy

The Hamiltonian for the S model given by Eq. (17) is effectively a single electron coupled to a single-boson-mode model similar to the model we studied for an electron-phonon coupled system in Refs. 59 and 60. We can then use the NEGF code we have developed to study the electronic properties of the S model for different levels of approximation for the corresponding self-energies. In the Feynman diagram language, these are given in Fig. 1 and correspond to (a) non-self-consistent calculations for the self-energy $\Sigma = G_0 W_p$, where G_0 is the core-electron bare Green's function and W_p is the plasmon propagator given in Eq. (12), (b) self-consistent calculations for the core electron Green's function $\Sigma = GW_p$, and to vertex corrections taken at the $\Gamma_{(1)}$ level of approximation for (e) non-self-consistent calculations $\Sigma = G\Gamma_{(1)}^{GW} W_p$ with G and $\Gamma_{(1)}^{GW}$ taken at the GW_p level, and (f) fully self-consistent $\Sigma = G\Gamma_{(1)}^{\text{SC}} W_p$ calculations.

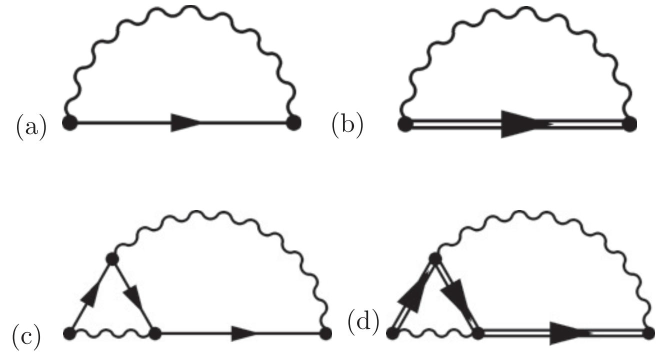

FIG. 1. Different levels of approximation for the one-particle self-energy $\Sigma = \Sigma^{(1)} + \Sigma^{(2)}$ within the plasmon model. First-order diagrams: (a) $\Sigma^{(1)} = G_0 W_p$ with G_0 being the bare core-electron Green's function, and (b) $\Sigma^{(1)} = GW_p$ for self-consistent calculations. Second-order diagrams with vertex corrections (c) $\Sigma^{(2)} = G\Gamma_{(1)}^{GW} W_p$ for non-self-consistent calculations, and (d) $\Sigma^{(2)} = G\Gamma_{(1)}^{\text{SC}} W_p$ for the full self-consistent calculations (see Appendix C2).

Our NEGF code, presented in Ref. 59 is versatile. It was originally developed to deal with an electron-phonon coupled system in contact with two electron reservoirs each at their own equilibrium. But the code can deal with any model Hamiltonian of electron-boson coupled systems. In the following, we use this code and we consider the whole system at equilibrium, and at zero or finite temperature. As explained above, the exact solution of the S model exists only for the equilibrium condition.

Additionally, we use an extremely small coupling constant to the reservoirs in order to introduce a finite but very small broadening in the spectral features of the S-model Hamiltonian (17) in a simple way (η has a tiny but finite numerical value). The details for the calculations of the different NEGF, at equilibrium and out of equilibrium, are given in Ref. 59.

In Ref. 59, we discussed the first and second-order diagrams for the electron-phonon interaction—topologically speaking, this will look similar to the GW-like self-energy diagrams we consider here (see Fig. 1), however, there the boson line is the phonon propagator and not the screened Coulomb interaction W with which we are concerned here. Furthermore, the parameters of the core electron-plasmon coupled system are given here by a single physical quantity: the electron density (see Table I).

D. Results

Within our model, all the characteristics of the plasmon are determined by a single parameter: the electron density or equivalently by the Wigner-Seitz radius r_S. There is then

TABLE I. Values (in atomic units) of the different relevant parameters, electron density n, Fermi energy ε_F, plasmon energy ω_p, electron-plasmon coupling constant γ_0, and relaxation energy D for different values of r_S.

r_S	5.0	4.0	3.0	2.0
n	0.00191	0.00373	0.00884	0.02984
ε_F	0.0737	0.1151	0.2046	0.4604
ω_p	0.1549	0.2165	0.3333	0.6124
ω_p^0	2.103	1.881	1.629	1.330
D	0.34046	0.31186	0.27789	0.23523
γ_0	0.22966	0.25985	0.30435	0.37953
γ_0/ω_p	1.48	1.20	0.91	0.62

only one other parameter left; the energy level ε_c of the core electron, which we take as being located one atomic unit of energy below the Fermi level ε_F of the different systems we consider.

Table I contains the values of the different relevant parameters for four different values of r_S. The high-density limit ($r_S = 2$) corresponds to a medium electron-plasmon coupling, while the low-density limit ($r_S = 5$) corresponds to a very strong electron-plasmon coupling.

Below, and in Figs. 2–5, we show results for the spectral function $A(\omega) = -\mathrm{i}[G^r(\omega) - G^a(\omega)]/2$ calculated at equilibrium for two values of r_S (medium coupling $r_S = 2$ and strong coupling $r_S = 4$) at zero and finite temperatures. We compare the exact results, Eq. (19), for the spectral function with the results obtained from the diagrammatic expansion of the self-energy and the vertex function shown in Fig. 1.

1. Exact results

The exact spectral function, calculated from the expression for the Green's function given in Eq. (19), is shown as a solid black line in Figs. 2 and 3. A broadening equal to the broadening of our NEGF calculations has been applied. Figure 2 shows the zero-temperature results for the high-density electron gas ($r_S = 2$). The exact result provided by Eq. (19) (solid black line) gives a spectral function with a peak localized at the renormalized core level $\tilde{\varepsilon}_c = \varepsilon_c + D$, and plasmon side-band peaks at $\tilde{\varepsilon}_c - n\omega_p$ ($n \geqslant 1$) corresponding to plasmon emission. The peaks are hence separated by the plasmon energy ω_p. In terms of amplitude, the main peak is that at $\tilde{\varepsilon}_c$ in the limit of weak to medium/strong electron-plasmon coupling, i.e., where $\gamma_0/\omega_p \leqslant 1$, and so for which $\gamma_0/\omega_p \leqslant 1$.

Figure 3 shows the zero-temperature results for stronger coupling, $r_S = 4$ and $\gamma_0/\omega_p > 1$. Now the renormalized core level $\tilde{\varepsilon}_C$ has shifted to $\omega/\omega_p \sim 1.5$, while the spectral weight is shifted toward lower energies and the main peak is now the plasmon side-band peak at around ω/ω_p.[61]

2. Diagrammatic expansion results

The main differences between the exact result and the diagrammatic expansions of the self-energies and of the vertex functions (as represented in Fig. 1) are as follows. First, let us discuss the results for the spectral functions in the high-density limit ($r_S = 2$) for which the electron-plasmon coupling is medium, $\gamma_0/\omega_p = 0.62$. The non-self-consistent

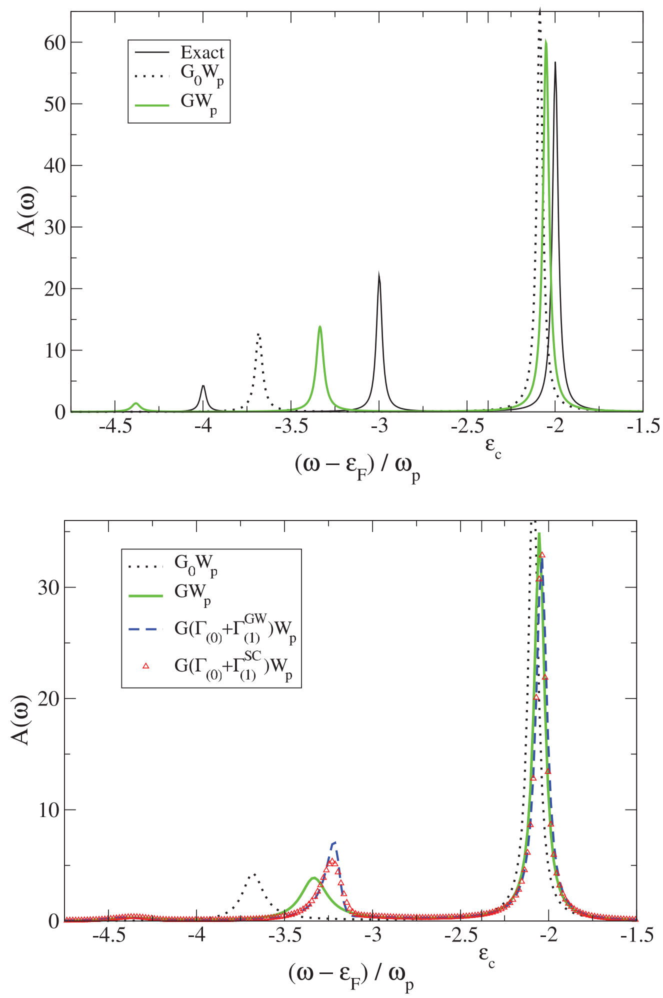

FIG. 2. (Color online) Zero-temperature equilibrium spectral functions $A(\omega)$ for the high-density limit with $r_S = 2$, corresponding to medium core electron-plasmon coupling $\gamma_0/\omega_p = 0.62$. Top panel: exact results and GW calculations with and without self-consistency $\Sigma = GW_p$, G_0W_p. Bottom panel: results for different levels of approximation for the self-energy $\Sigma = G_0W_p$, GW_p, $G(\Gamma_{(0)} + \Gamma_{(1)}^{GW})W_p$, and $G(\Gamma_{(0)} + \Gamma_{(1)}^{\mathrm{SC}})W_p$ (see Fig. 1) with fewer grid points ($N_\omega = 1579$), giving an extra broadening.

GW calculations [i.e., $\Sigma = G_0W_p$, Fig. 1(a), dotted black lines in Fig. 2] generate only two peaks, the renormalized core level with one plasmon side-band peak, as expected. However, the positions of those two peaks are incorrect.

The self-consistent GW calculations [i.e., $\Sigma = GW_p$, Fig. 1(b), solid green lines in Figs. 2 and 3] generate the correct series of plasmon side-band peaks. However, the corresponding relaxation energy D is too small and the energy position of the first plasmon side-band peak is too low. It should be noticed, however, that the energy separation between the plasmon side-band peaks is correctly reproduced, i.e., equal to ω_p.

For the low-density limit ($r_S = 4$) for which the electron-plasmon coupling is very strong, $\gamma_0/\omega_p = 1.20$, the GW calculations poorly describe the exact spectral density. The self-consistent GW calculations generate the correct series

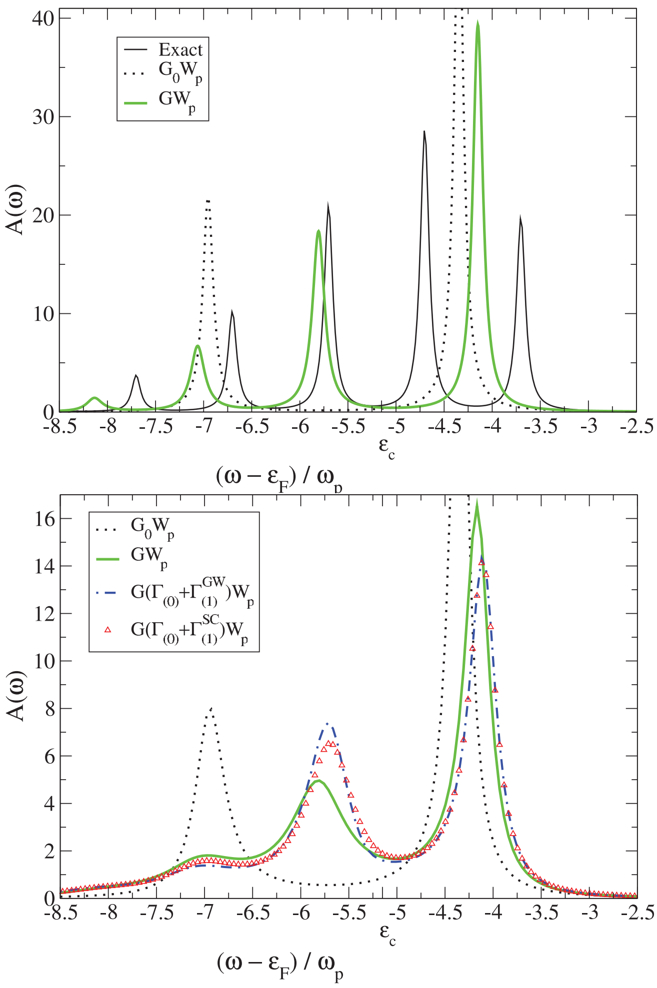

FIG. 3. (Color online) Zero-temperature equilibrium spectral functions $A(\omega)$ for the low-density limit with $r_S = 4$, corresponding to very strong core electron-plasmon coupling $\gamma_0/\omega_p = 1.20$. Top panel: exact results and *GW* calculations for the different self-energies $\Sigma = G_0W_p$, GW_p. Bottom panel: results for different levels of approximation for the self-energy $\Sigma = G_0W_p$, GW_p, $G(\Gamma_{(0)} + \Gamma_{(1)}^{GW})W_p$, and $G(\Gamma_{(0)} + \Gamma_{(1)}^{\mathrm{SC}})W_p$ (see Fig. 1) with fewer grid points ($N_\omega = 1579$), giving an extra broadening, in comparison to the top panel.

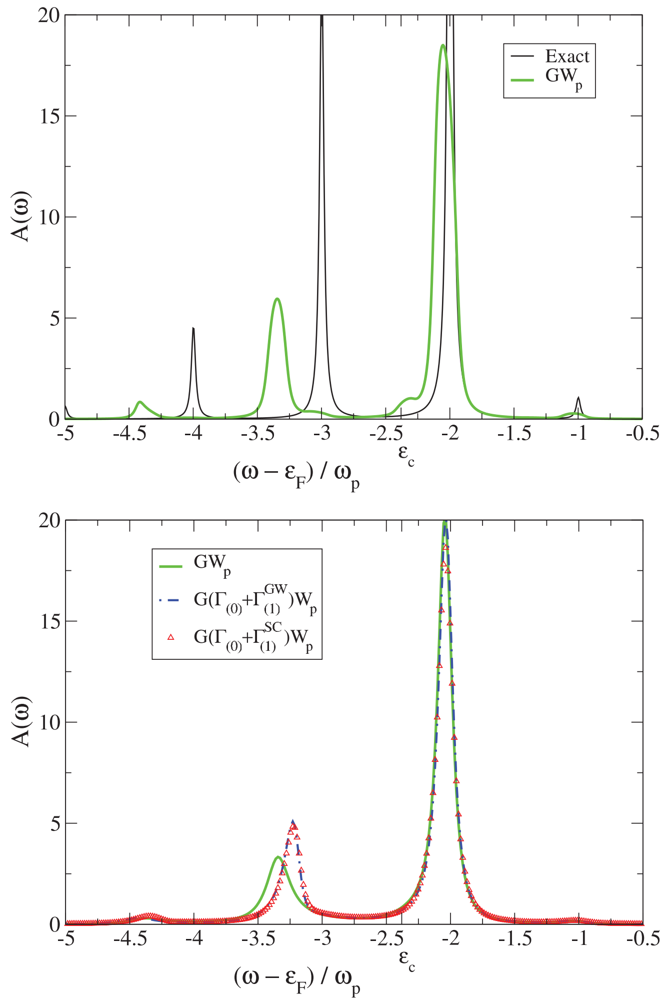

FIG. 4. (Color online) Finite-temperature equilibrium spectral functions $A(\omega)$ for the high-density electron gas with $r_S = 2$ and a finite temperature $kT = 0.2$ corresponding to $\omega_p/kT = 3.062$. Top panel: exact results and calculations for different self-energies $\Sigma = GW_p$ and $GW_p^{(2)\mathrm{SC}}$. Bottom panel: results for different self-energies $\Sigma = GW_p$, $G(\Gamma_{(0)} + \Gamma_{(1)}^{GW})W_p$, and $G(\Gamma_{(0)} + \Gamma_{(1)}^{\mathrm{SC}})W_p$ (see Fig. 1) with fewer grid points ($N_\omega = 1579$), giving an extra broadening.

of peaks but with a completely wrong weight distribution. This is unsurprising since the *GW* approach corresponds to a partial resummation of the diagrams, and does not include all other relevant diagrams necessary to deal with the very strong regime.

The lowest-order vertex corrections to the self-energy [Figs. 1(d) and 1(e), blue dashed lines and red triangles in Figs. 2 and 3] introduce modifications of the peak positions. They generate a slightly better relaxation energy D and a shift of the side-band peaks toward the renormalized electron core level (Figs. 2 and 3, bottom panels). Vertex corrections globally improve the spectral information toward better overall agreement with the exact results. However, the lowest-order vertex correction expansion $\Gamma_{(0)} + \Gamma_{(1)}$ (see Appendix C) is still not sufficiently good to qualitatively reproduce the exact spectral functions in the limit of very strong electron-plasmon coupling.

The fully self-consistent calculations with $G\Gamma_{(1)}^{\mathrm{SC}}W_p$ seem to only marginally affect the line shape of the plasmon side-band peaks in comparison to their non-self-consistent counterpart. Note that a fine analysis of the comparison between the exact results and the diagrammatic perturbation results with vertex correction is difficult to perform in Figs. 2 and 3, as the calculations were done for different numbers of ω-grid points N_ω. It was necessary to perform the calculations in that way because the vertex corrections scale as N_ω^3 as shown in Ref. 59. Therefore we have performed the corresponding calculations with a lower number of points $N_\omega = 1579$ for the bottom panels of Figs. 2 and 3, instead of $N_\omega = 16\,385$ points for the top panels, in order to have tractable computational costs. Our NEGF code works with a finite broadening related to the number of grid points to deal with sharply peaked and/or discontinuous functions, hence the different line shape in the spectral functions in the top and bottom panels of Figs. 2 and 3, respectively. This numerical extra broadening affects

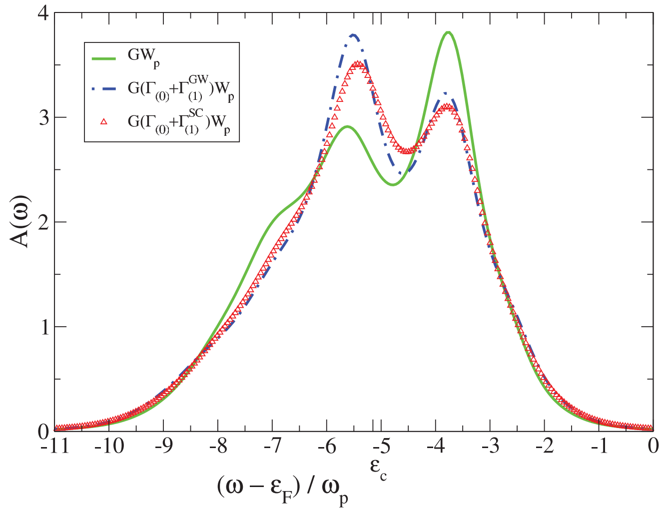

FIG. 5. (Color online) Finite-temperature equilibrium spectral functions $A(\omega)$ for the low-density electron gas with $r_S = 4$ and a finite temperature $kT = 0.2$ (corresponding to $\omega_p/kT = 1.083$) and with fewer grid points $N_\omega = 1579$. Calculations for different self-energies $\Sigma = GW_p$, $GW_p^{(2)\mathrm{SC}}$, $G(\Gamma_{(0)} + \Gamma_{(1)}^{GW})W_p$, and $G(\Gamma_{(0)} + \Gamma_{(1)}^{\mathrm{SC}})W_p$ (see Fig. 1) are shown.

only the width of the peaks and the global amplitude of the spectral functions, though all spectral functions are always normalized. There is no major problem with the spectral information contained in $A(\omega)$. We have discussed in detail the effects of this extra broadening in Ref. 59.

In addition, we want to add that our results confirm those obtained in earlier studies, see, for example, Refs. 38,39,45 and 62. However, our self-consistent scheme for calculating the second-order diagrams by starting with the GW-like Green's function allows us to avoid the problem of negative spectral densities (at least within the range of parameters we have explored) that were obtained in Refs. 39,62, and 63.

3. Finite temperatures

For finite temperatures, the exact result provided by Eq. (19) can be generalized from a thermodynamical average over the boson statistics within a canonical ensemble.[58,61] In addition to the peaks at $\tilde{\varepsilon}_c - n\omega_p$ ($n \geqslant 0$), one also sees spectral information at $\tilde{\varepsilon}_c + n\omega_p$ ($n \geqslant 1$) that corresponds to absorption of the thermally populated plasmons, as shown in Fig. 4.

The results for the spectral functions obtained from the diagrammatic expansion of the self-energy and of the vertex functions as shown in Fig. 1 are shown in Figs. 4 and 5. Qualitatively, we obtain similar effects of the second-order diagrams on the spectral functions as in the case of zero temperature. Note that, however, for finite temperatures, the dependence of the line shape upon the extra broadening related to the number of ω-grid points is much less important, since the thermal broadening is dominating. In Fig. 4, we see that, as for the zero-temperature case, the self-consistent GW_p calculations generate the correct series of peaks with the plasmon emission sideband peaks again appearing at too low energies. However, the new plasmon absorption peak just above the main peak is almost at the correct energy position.

We do not yet have an accurate explanation for the tiny shoulder-like feature around the Fermi level in the top panel of Fig. 4. However, this feature is related to plasmon absorption processes since at the chosen temperature the plasmon mode can be thermally populated. Nonetheless, it is clear that the feature disappears when performing the calculations with an extra broadening (i.e., introducing an effective finite lifetime for the plasmon mode). When we consider the strong coupling case, shown in Fig. 5, we find that for all levels of approximation the line shape is strongly broadened, washing out most of the features.

We can conclude that, within the limit of the S model and for both the zero-temperature and finite-temperature cases, the various GW approximations are much more accurate for the high-density regime. For the low-density electron gas, both the GW peak positions and line shapes are poor in comparison to the exact results, although the separation between the plasmon sideband peaks is correctly reproduced.

E. Spectral function of pure jellium and vertex corrections

In this section, we compare different approximations for the vertex corrections for another model system: the pure jellium model (without a distinct core level). The spectral functions in this system are evaluated in the zero-temperature limit within conventional Green's functions calculations.[64]

It is expected from the original work of Hedin *et al.*[3] and also of Shirley[45] that the exact spectral function of pure jellium should show several plasmon resonances below the main quasiparticle peak. However, we do not observe any such peaks (see Fig. 6) when iterating the Green's function to self-consistency within the GW approximation or when we use model vertex corrections.[5,45] These vertex corrections were, however, supposed to provide an exact description of screened Coulomb interaction W for the jellium model.

Any self-consistent iteration has the effect of broadening the occupied bandwidth (a feature that is known to be unphysical) as evidenced by the shift in the main quasiparticle peak at the bottom of the band seen in Fig. 6. The model vertex corrections tested do not remedy this behavior, nor do they lead to any multiplasmon resonances. We consider two different models for the vertex corrections: firstly, a strictly local vertex correction applied in the screening, annotated $\tilde{W}_0$ and modeled directly by the LDA exchange-correlation kernel as described by Del Sole *et al.*[5] Secondly, the other vertex correction incorporates a momentum-dependent local-field factor modelled on exact quantum Monte Carlo results for jellium, as described by Shirley[45] (annotated W_{S}).

In general, the difference between the two different types (static versus q dependent) of vertex corrections implemented is practically negligible in the spectral functions. This shows that the screened interaction can be very insensitive to the exact type of vertex correction used, in contrast to the self-energy. With a self-consistent calculation, we also observe the broadening of spectral peaks previously noted in Refs. 44 and 47.

This also indicates that the explicit evaluation of the second-order diagrammatic vertex correction, $\Gamma_{(1)}$, is imperative in order to capture the higher-order plasma satellites in a metallic system, and in corresponding models with a coupling to a

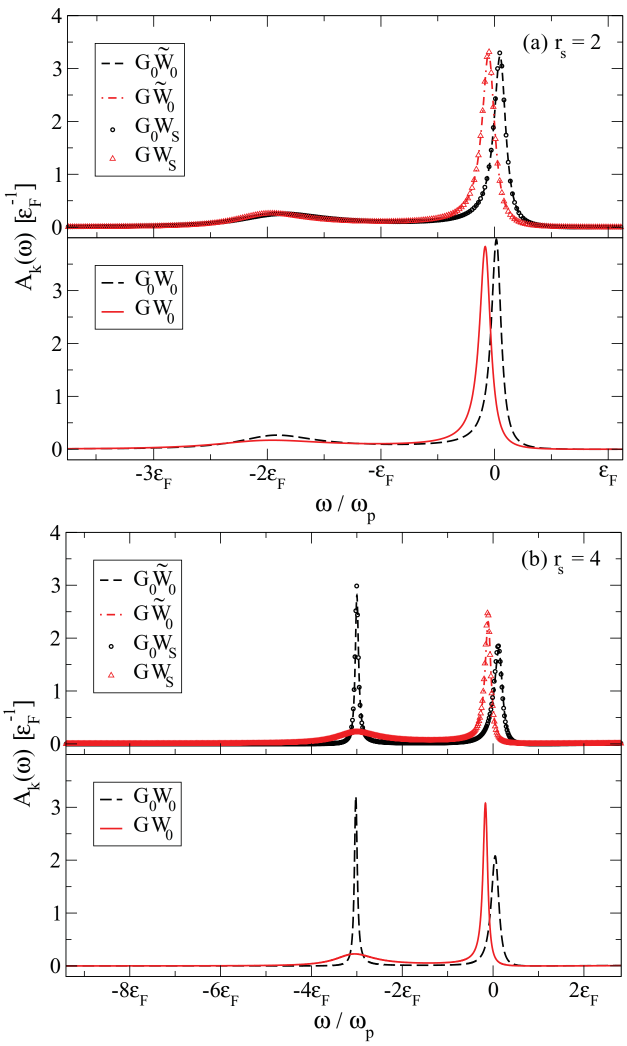

FIG. 6. (Color online) Spectral function $A_k(\omega)$ at $k = 0$ and for (a) $r_S = 2$ and (b) $r_S = 4$ for the pure jellium model. Each set of curves shows a one-shot calculation for G_0 (black dash curves) and self-consistent iterations for G (red solid curves). The bottom panel of plots (a) and (b) show standard G_0W_0 and GW_0, the top panels show $G_0\tilde{W}_0$ and $G\tilde{W}_0$ with a local vertex correction in $\tilde{W}_0$ as described in Ref. 5. G_0W_S and GW_S refer to a momentum-dependent vertex correction in W_S defined in Ref. 45 to approximate the exact W of jellium. The results including the different vertex corrections are indicated with a line (for $\tilde{W}_0$) and a symbol (for W_S). All chemical potentials are aligned at the Fermi energy ϵ_F of the noninteracting gas. The positive (negative) deviation of the main quasiparticle peak from the origin indicates a narrowing (broadening) of the occupied bandwidth. None of these approximations provides more than one plasmon satellite in contrast to the expected exact result.

core state as shown in the previous section. This finding is fully consistent with the previous work of Shirley[45] where the vertex function $\Gamma_{(1)}$ was approximately evaluated within the zero-temperature formalism.

V. CONCLUSIONS

We have formally expressed the Hedin's GW equations on the Keldysh time-loop contour. This implies that within our formalism one can now deal with full nonequilibrium conditions for fully interacting electron systems. The equilibrium properties of the system are obtainable from our formalism as a special case of the more general nonequilibrium conditions.

We have considered in particular the lowest-order expansions of the electron self-energy Σ and of the vertex function Γ, and compared our results with previous work. We have then used our formalism to study a simple model of an electron core level coupled to a plasmon mode for which exact results for the spectral function are available (i.e., the S model). We have compared our lowest-order expansions of the electron self-energy and of the vertex function with the exact results, considering the second-order diagrams in terms of the plasmon propagator W_p.

We have shown that self-consistent GW-based approximations (with or without vertex corrections) provide a good approximation to the exact results in the limit of weak-to-medium electron-plasmon coupling (i.e., high electron-density limit) both at zero and finite temperatures. Non-self-consistent G_0W_p calculations do not reproduce the complete series of plasmon sattelites. However, the GW-based approximations perform quite poorly in the strong-coupling limit (i.e., low electron-density limit). Vertex corrections generally readjust the peak positions (the relaxation energy responsible for the renormalization of the core level as well as the plasmon side-band peaks) toward the correct result.

Furthermore, we have also analyzed the spectral functions obtained from conventional equilibrium GW calculations for the pure jellium model and using different approximation for the vertex corrections in W. The corresponding results confirm that the explicit second-order diagrams for the vertex corrections are needed to obtain the full series of plasmon side-band resonances.

In appendix D, we have also addressed an important issue about the Dyson-like equation for the time-ordered Green's function in the energy representation. We have shown that there is a difference between Dyson equation for the Green's function obtained at zero temperature and at finite temperature, as already pointed out in Ref. 3. We have shown that at finite temperature there are extra terms in the Dyson equation of the time-ordered Green's function. These terms are obtained rigorously from the Keldysh time-loop formalism we derived at equilibrium, while they were introduced *ad hoc* by Hedin and Lundqvist[3] to recover an exact result.

Finally, we have studied in this paper models of interacting electron systems, but we believe that our theoretical approach is well suited for applications toward more realistic physical systems, such as the one-dimensional plasmon modes recently observed in an atomic-scale metal wire deposited on a surface.[70]

ACKNOWLEDGMENTS

We gratefully acknowledge Pablo García González for useful discussions, comments, and the use of a version of his jellium code. This work was funded in part by the European Community's Seventh Framework Programme (FP7/2007-2013) under grant agreement No. 211956 (ETSF e-I3 grant).

APPENDIX A: RELATIONSHIP BETWEEN THE DIFFERENT GREEN'S FUNCTIONS AND SELF-ENERGIES

The relations between the different components of the Green's functions and self-energies on the Keldysh time-loop contour are given as usual, with $X^{\eta_1\eta_2}(12) \equiv G^{\eta_1\eta_2}(12)$ or $\Sigma^{\eta_1\eta_2}(12)$.

$$\begin{aligned} X^r &= X^{++} - X^{+-} = X^{-+} - X^{--},\\ X^a &= X^{++} - X^{-+} = X^{+-} - X^{--},\\ X^{++} &+ X^{--} = X^{+-} + X^{-+},\\ X^{-+} &- X^{+-} = X^r - X^a. \end{aligned} \tag{A1}$$

The usual lesser and greater projections are defined respectively as $X^< \equiv X^{+-}$ and $X^> \equiv X^{-+}$, and the usual time ordered (anti-time ordered) as $X^t = X^{++}$ ($X^{\tilde{t}} = X^{--}$).

APPENDIX B: RULES FOR ANALYTICAL CONTINUATION

For the following products $P_{(i)}(\tau,\tau')$ on the time-loop contour C_K:

$$\begin{aligned} P_{(2)} &= \textstyle\int_{C_K} AB,\\ P_{(3)} &= \textstyle\int_{C_K} ABC,\\ P_{(n)} &= \textstyle\int_{C_K} A_1 A_2 ... A_n, \end{aligned}$$

we have the following rules for the different components $P^x_{(i)}(t,t')$ on the real-time axis: ($x = r,a, >, <$)

$$\begin{aligned} P^{\gtrless}_{(2)} &= \textstyle\int_t A^r B^{\gtrless} + A^{\gtrless} B^a,\\ P^<_{(3)} &= \textstyle\int_t A^< B^a C^a + A^r B^< C^a + A^r B^r C^<,\\ P^r_{(n)} &= \textstyle\int_t A^r_1 A^r_2 \dots A^r_n\,, \qquad P^a_{(n)} = \int_t A^a_1 A^a_2 \dots A^a_n. \end{aligned}$$

APPENDIX C: LOWEST-ORDER EXPANSION OF THE VERTEX FUNCTION $\Gamma(12;3)$

1. The $\Gamma_{(0)}$ level of approximation: no vertex corrections

In this section, we derive from our general results, the more conventional GW approach used in previous studies on the ground-state properties of molecules, semiconductors, or on the linear response, or the full nonequilibrium transport properties of nanoscale systems driven by an applied external voltage.[28,33,34,71–75]

With no vertex corrections, $\Gamma(12;3)$ is simply given by $\Gamma_{(0)}(12;3) = \delta(12)\delta(13)$. Hence the polarizability $\tilde{P}(12)$ and the electron self-energy $\Sigma(12)$ are

$$\tilde{P}(12) = -\mathrm{i}G(12)\, G(21), \tag{C1}$$

$$\Sigma(12) = \mathrm{i}G(12)\, W(21).$$

The different components of the polarizability are then

$$\tilde{P}^{\lessgtr}(12) = -\mathrm{i}G^{\lessgtr}(12)\, G^{\gtrless}(21). \tag{C2}$$

Using Eq. (A1), we find that the retarded polarizability is given by

$$\begin{aligned} \tilde{P}^r(12) &= -\mathrm{i}[G(12)\, G(21)]^r\\ &= -\mathrm{i}G^r(12)\, G^<(21) - \mathrm{i}G^<(12)\, G^a(21) \end{aligned} \tag{C3}$$

and the electron self-energy by

$$\begin{aligned} \Sigma^<(12) &= \mathrm{i}G^<(12)\, W^>(21),\\ \Sigma^r(12) &= \mathrm{i}[G(12)\, W(21)]^r\\ &= \mathrm{i}G^r(12)\, W^<(21) + \mathrm{i}G^<(12)\, W^a(21). \end{aligned} \tag{C4}$$

Using the symmetry relations for W and Eq. (A1), we can easily recast the above equations in the following form:

$$\begin{aligned} \Sigma^<(12) &= \mathrm{i}G^<(12)\, W^<(12),\\ \Sigma^r(12) &= \mathrm{i}G^r(12)\, W^>(12) + \mathrm{i}G^<(12)\, W^r(12). \end{aligned} \tag{C5}$$

These expressions for Σ and $\tilde{P}$ are just the equivalent of Eqs. (3)–(8) in Ref. 33 and are similar to the corresponding expressions in Refs. 31,32, 28, and 34.

2. The $\Gamma_{(1)}$ level of approximation

With the series expansion $\Gamma(12;3) = \sum_n \Gamma_{(n)}(12;3)$ in which the index n represents the number of times the screened Coulomb interaction W appears explicitly in the series, we take for $\Gamma_{(1)}(12;3)$:

$$\Gamma_{(1)}(12;3) = \int \mathrm{d}(4567)\, \frac{\delta\Sigma(12)}{\delta G(45)} G(46)G(75)\Gamma(67;3), \tag{C6}$$

where $\Gamma(67;3) = \Gamma_{(0)}(67;3) = \delta(67)\delta(63)$ and $\Sigma = \mathrm{i}GW$. Hence $\Gamma_{(1)}(12;3) = \mathrm{i}W(21)\, G(13)\, G(32)$.

In the following, we derive the part of the electron self-energy and the part of the polarizability arising from $\Gamma_{(1)}$ only. In principle, the full Σ and $\tilde{P}$ should be calculated by using $\Gamma = \Gamma_{(0)} + \Gamma_{(1)}$. We find for the electron self-energy (defined on the contour C_K),

$$\begin{aligned} \Sigma(12) &= \mathrm{i} \int \mathrm{d}(34)\, G(13)\, \Gamma_{(1)}(32;4)\, W(4,1)\\ &= \mathrm{i} \times \mathrm{i} \int \mathrm{d}(34)\, G(13)\, W(23)\, G(34)\, G(42)\, W(41). \end{aligned} \tag{C7}$$

The different components $\Sigma^{\eta_1\eta_2}$ of the self-energy on the time-loop contour (with $\eta_{1,2} = \pm$) are then given by

$$\begin{aligned} \Sigma^{\eta_1\eta_1}(12) = -\sum_{\eta_3\eta_4} \eta_3\eta_4 \int \mathrm{d}(34)\, & G^{\eta_1\eta_3}(13)\, W^{\eta_2\eta_3}(23)\\ & \times G^{\eta_3\eta_4}(34)\, G^{\eta_4\eta_2}(42)\, W^{\eta_4\eta_1}(41). \end{aligned} \tag{C8}$$

This self-energy corresponds to the so-called double-exchange diagram. Note that we have studied the effects of such a diagram in the different context of a propagating electron coupled to a local vibration mode, in which the bosonic propagator W is replaced by a phonon propagator D.[59]

At the $\Gamma_{(1)}$ level of approximation, we find that the polarizability is given by

$$\tilde{P}(12) = -\mathrm{i} \int \mathrm{d}(34)\, G(13)\, G(41)\, \Gamma_{(1)}(34;2) = \int \mathrm{d}(34)\, G(13)\, G(41)\, W(43)\, G(24)\, G(32), \quad \text{(C9)}$$

with components on C_K given by

$$\tilde{P}^{\eta_1\eta_2}(12) = \sum_{\eta_3\eta_4} \eta_3\eta_4 \int \mathrm{d}(34) G^{\eta_1\eta_3}(13)\, G^{\eta_4\eta_1}(41) \times W^{\eta_4\eta_3}(43)\, G^{\eta_2\eta_4}(24)\, G^{\eta_3\eta_2}(32). \quad \text{(C10)}$$

Here again, and as well as for the self-energy, the retarded (advanced) part $\tilde{P}^r(12)$ is obtained from $\tilde{P}^r = \tilde{P}^{++} - \tilde{P}^{+-}$. One can then express $\tilde{P}^r$ and $\tilde{P}^{+-}$ in a more compact form involving only terms like $X^{r,a,\lessgtr}$ (with $X \equiv G, W$).

APPENDIX D: TIME-ORDERED GREEN'S FUNCTIONS AT EQUILIBRIUM

In this section, we discuss in detail the relation between time-ordered Green's function (in energy representation) for two temperature limits. Differences are expected to arise as shown in Chap. IV.17. of Ref. 3. We use the conventional equilibrium many-body perturbation theory (MBPT) to determine the time-ordered Green's function G^t, and the generalization of the Green's function onto the Keldysh time-loop contour at equilibrium to determine the counterpart of the time-ordered Green's function G^{++}.

From MBPT, the time-ordered Green's function satisfies the Dyson-like equation $G^t = g^t + g^t \Sigma^t G^t$ and the corresponding time-ordered Green's function obtained from the Keldysh time-loop expansion satisfies the corresponding Dyson-like equation $G^{++} = g^{++} + (g\Sigma G)^{++}$. In principle, from the conventional definition, we have $g^t = g^{++}$ and should have $G^t = G^{++}$.

It is easy to show that from the rules of analytical continuation, $G^{++} = g^{++} + (g\Sigma G)^{++}$ is expanded as follows:

$$G^{++} = g^{++} + g^{++}\Sigma^{++}G^{++} - g^{++}\Sigma^{<}G^{>} + g^{<}\Sigma^{>}G^{++} + g^{<}\Sigma^{--}G^{++}, \quad \text{(D1)}$$

and after further manipulation [using the notation $(g/G)^t = (g/G)^{++}$],

$$G^t = g^t + (g^t\Sigma^t - g^{<}\Sigma^{>})G^t - (g\Sigma)^{<}G^{>}. \quad \text{(D2)}$$

So, strictly speaking, the nonequilibrium formalism introduces two extra terms $g^{<}\Sigma^{>}G^t$ and $(g\Sigma)^{<}G^{>}$ in the Dyson equation for G^t.

We now analyze these two terms in more detail. First of all, we recall that at equilibrium or in a steady state, the Green's functions and self-energies depend only on the time difference of their argument and can be Fourier transformed with a single energy argument. We then have the following expression:

$$G^t(\omega) = g^t(\omega) + [g^t(\omega)\Sigma^t(\omega) - g^{<}(\omega)\Sigma^{>}(\omega)]G^t(\omega) - (g\Sigma)^{<}(\omega)G^{>}(\omega). \quad \text{(D3)}$$

Furthermore, at equilibrium or in a steady state, the lesser and greater components of either a Green's function or a self-energy ($X^{\lessgtr}$) can be expressed in terms of the corresponding advanced and retarded quantity and a distribution function,[65–68] i.e.,

$$X^{\lessgtr}(\omega) = -f^{\lessgtr}(\omega)[X^r(\omega) - X^a(\omega)]. \quad \text{(D4)}$$

At equilibrium, $f^{\lessgtr}(\omega) = f_0^{\lessgtr}(\omega)$ and for a system of fermions, $f_0^{<}$ is given by the Fermi-Dirac distribution function $f^{\mathrm{eq}}(\omega) = 1/[1 + \exp\beta(\omega - \mu^{\mathrm{eq}})]$ and $f_0^{>} = f^{\mathrm{eq}} - 1$ (with $\beta = 1/kT$).

At zero temperature, the Fermi-Dirac distribution takes only two different values, $f^{\mathrm{eq}} = 1$ or 0. Hence we have the property $(f^{\mathrm{eq}})^2 = f^{\mathrm{eq}}$, which implies that $f_0^{<}(\omega) f_0^{>}(\omega) = f^{\mathrm{eq}}(f^{\mathrm{eq}} - 1) = 0$. Consequently, any products of the kind $X^{<}(\omega)Y^{>}(\omega)$ or $X^{>}(\omega)Y^{<}(\omega)$ vanish. Therefore we recover from the Keldysh time-loop formalism Eq. (D3) at zero temperature, the conventional Dyson equation $G^t = g^t + g^t\, \Sigma^t\, G^t$ as expected. At finite temperature, $f_0^{<}(\omega) f_0^{>}(\omega) = f^{\mathrm{eq}}(f^{\mathrm{eq}} - 1) = kT\partial_\omega f^{\mathrm{eq}} \neq 0$, and the product $f_0^{<} f_0^{>}$ gives a sharply peaked function at the Fermi level $\mu^{\mathrm{eq}} = \varepsilon_F$ with a width of approximately kT.

We now check the individual contribution of each term $g^{<}\Sigma^{>}$ and $(g\Sigma)^{<}G^{>}$, first for a specific case (i.e., the quasiparticle approximation) and then for the general case. In a quasiparticle scheme, i.e., when a single index k is good enough to represent the quantum states (with energy ε_k), the Green's functions and the self-energies in the absence and in the presence of interaction are diagonal in this representation. We have

$$g_k^{<}(\omega)\Sigma_k^{>}(\omega) = -f_{0,k}^{<}\big(g_k^r - g_k^a\big)(\omega) \times -f_{0,k}^{>}\big(\Sigma_k^r - \Sigma^a\big)(\omega) = 4\pi f_{0,k}^{<} f_{0,k}^{>} \delta(\omega - \varepsilon_k)\, \Im m\, \Sigma_k^r(\omega). \quad \text{(D5)}$$

For purely fermionic systems at equilibrium, one usually has $\Im m\, \Sigma_k^r(\mu^{\mathrm{eq}}) = 0$,[11] and therefore $g_k^{<}(\mu^{\mathrm{eq}})\Sigma_k^{>}(\mu^{\mathrm{eq}}) = 0$. When $\Im m\, \Sigma_k^r$ also vanishes in the energy window around the Fermi level, defined by $f_0^{<} f_0^{>} \neq 0$, then the product $g_k^{<}(\omega)\Sigma_k^{>}(\omega)$ also vanishes. When there are no eigenvalues ε_k (of the noninteracting system) within this energy window, then once more, we have $g_k^{<}(\omega)\Sigma_k^{>}(\omega) \sim 0$. Otherwise, $g_k^{<}(\omega)\Sigma_k^{>}(\omega) = \tilde{Z}_k \delta(\omega - \varepsilon_k)$ with $\tilde{Z}_k = 4\pi[f_0^{<} f_0^{>} \Im m\, \Sigma_k^r(\omega)]_{\omega=\varepsilon_k}$.

For the second correction term, we have

$$(g\Sigma)_k(\omega)^{<} G_k^{>}(\omega) = -f_{0,k}^{<}\big[(g\Sigma)_k^r - (g\Sigma)_k^a\big](\omega) \times -f_{0,k}^{>}\big(G_k^r - G_k^a\big)(\omega) = f_{0,k}^{<}\big(g_k^r\Sigma_k^r - g_k^a\Sigma_k^a\big)(\omega)\, f_{0,k}^{>}\big(G_k^r - G_k^a\big)(\omega). \quad \text{(D6)}$$

For the quasiparticle scheme, $\Im m\, \Sigma_k^{r/a} \sim \pm \mathrm{i}\eta$ around the Fermi level $\mu^{\mathrm{eq}} \pm kT$, and we find that

$$(g_k\Sigma_k)^{<} G_k^{>} = -4\pi f_0^{<} f_0^{>} Z_k \Re e\, \Sigma_k^r(\varepsilon_k)\, \delta(\omega - \varepsilon_k)\delta(\omega - \tilde{\varepsilon}_k), \quad \text{(D7)}$$

with $Z_k^{-1} = 1 - (\partial \Re e\Sigma_k^r/\partial\omega)_{\omega=\tilde{\varepsilon}_k}$ being the effective mass renormalization parameter and $\tilde{\varepsilon}_k = \varepsilon_k + \Re e\Sigma_k^r$ being the renormalized eigenvalue. Hence the product $(g_k\Sigma_k)^{<}G_k^{>}$ vanishes because, in general, one has $\tilde{\varepsilon}_k \neq \varepsilon_k$. In the opposite case, when $\tilde{\varepsilon}_k = \varepsilon_k$ for some quantum states, the product $(g_k\Sigma_k)^{<}G_k^{>}$ also vanishes because then $\Re e\Sigma_k^r = 0$. Therefore our analysis shows that, in the quasiparticle scheme at finite temperature, Eq. (D3) reduces to the conventional Dyson equation $G_k^t = g_k^t + g_k^t\, \Sigma_k^t\, G_k^t$ as expected.

Now we need to check what is happening to the two contributions $g^<\Sigma^>$ and $(g\Sigma)^<G^>$ beyond the quasiparticle approximation. For that we can proceed further by going back to the full time dependence of Eq. (D2) and factorizing the noninteracting time-ordered Green's function g^t:

$$G^t = g^t\{1 + [\Sigma^t - (g^t)^{-1}g^<\Sigma^>]G^t - (g^t)^{-1}(g\Sigma)^<G^>\}, \tag{D8}$$

with $(g\Sigma)^< = g^<\Sigma^a + g^r\Sigma^<$. By using the equation of motion of the noninteracting time-ordered Green's function g^t,

$$\left[\mathrm{i}\frac{\partial}{\partial t_1} - h_0(1)\right]g^t(12) = \delta(12), \tag{D9}$$

it is straightforward to find that

$$(g^t)^{-1}(13) = \left[\mathrm{i}\frac{\partial}{\partial t_1} - h_0(1)\right]\delta(13). \tag{D10}$$

and, consequently,

$$\begin{aligned}(g^t)^{-1}g^<(14) &\equiv \int \mathrm{d}3\ (g^t)^{-1}(13)g^<(34)\\ &= \left[\mathrm{i}\frac{\partial}{\partial t_1} - h_0(1)\right]g^<(14) = 0,\end{aligned} \tag{D11}$$

the last equality comes from the definition of $g^<(14)$. Similarly, one can find that $(g^t)^{-1}g^r \equiv \int \mathrm{d}3\ (g^t)^{-1}(13)g^r(34) = \delta(14)$. Hence Eq. (D8) is transformed into

$$G^t = g^t + g^t\Sigma^t G^t - \Sigma^<G^>, \tag{D12}$$

where the last term, $\Sigma^<G^>$, satisfies the detailed balance equation at equilibrium:[16] $\Sigma^<G^> = \Sigma^>G^<$.

Equation (D12) is the most general expression for G^t and is the most important result of this section. It is interesting to note that Eq. (D12) is the equivalent of Eq. (17.9) derived in Ref. 3. However, in our approach, the extra term $\Sigma^<G^>$ is obtained rigorously from the use of the general Keldysh time-loop contour formalism. While in Ref. 3, Hedin and Lundqvist introduced this correction term *ad hoc* in the Dyson equation for the finite-temperature time-ordered Green's function in order to recover the proper limit of the independent particle case.

Once more, one can show that, after Fourier transforming, the product $\Sigma^<G^>$ vanishes at equilibrium and at zero temperature because of Eq. (D3) and $f_0^< f_0^> = 0$. Within the quasiparticle scheme at finite temperature, we have $\Sigma_k^<(\omega)G_k^>(\omega) = -4 f_{0,k}^< f_{0,k}^>\ \Im m\Sigma_k^r(\omega)\ \Im m G_k^r(\omega)$. Thus one needs to check the contributions of the spectral information in $\Im m\Sigma_k^r(\omega)$ and in $\Im m G_k^r(\omega)$ (in the energy window defined by $f_{0,k}^< f_{0,k}^>$ around the Fermi level) to see if the product $\Sigma_k^< G_k^>$ vanishes (as shown above).

We conclude this appendix by saying that there is indeed a difference between the Dyson equations for the time-ordered Green's functions at zero and finite temperature.[3,69,76] This result by no means contradicts the fact that the Green's functions on the Keldysh contour, the time-ordered Green's function at zero-temperature and the Matsubara-temperature Green's function of imaginary argument all obey the same formal Dyson equation. Our derivations provide a rigorous mathematical result for the finite-temperature time-ordered Green's function (in the energy representation) that satisfies a Dyson equation with an extra term as introduced in an *ad hoc* way in Chap. IV.17 of Ref. 3.

In our calculations, the correction term $\Sigma^<G^>$ is automatically taken into account, since we work with the Keldysh time-loop formalism. We have checked numerically that the $\Sigma^<G^>$ indeed vanishes at zero temperature. For finite temperatures, we have found that $\Sigma^<G^> \sim 0$ in the energy window defined by $f_0^< f_0^> \neq 0$ since most of the spectral weight is far below the Fermi level (see Figs. 2 to 5). However, in the limit of very high temperatures (i.e., $\omega_p/kT \ll 1$), the energy window defined by $f_0^< f_0^> \neq 0$ is wide and the product $\Sigma^<G^>$ does not vanish; though the corrections are two orders of magnitude smaller than the amplitude of the Green's function G^t itself.

It would be interesting to find real cases of interacting electron systems (probably of low dimensionality) for which the correction term $\Sigma^<G^>$ is not negligible. At finite but low temperatures, systems with a strong spectral density around the Fermi level (i.e., presenting the Kondo effect) at low temperature should be a good example. The high-temperature limit for metallic systems represents another interesting case as shown, for example, in Ref. 11.

*herve.ness@york.ac.uk

[1] A. A. Abrikosov, L. P. Gorkov, and I. E. Dzyaloshinski, *Methods of Quantum Field Theory in Statistical Physics* (Dover, New York, 1963).
[2] L. Hedin, Phys. Rev. **139**, A796 (1965).
[3] L. Hedin and S. Lundqvist, in *Solid State Physics* (Academic, New York, 1969), Vol. 23.
[4] R. W. Godby, M. Schlüter, and L. J. Sham, Phys. Rev. B **37**, 10159 (1988).
[5] R. Del Sole, L. Reining, and R. W. Godby, Phys. Rev. B **49**, 8024 (1994).
[6] F. Aryasetiawan and O. Gunnarsson, Rep. Prog. Phys. **61**, 237 (1998).
[7] M. M. Rieger, L. Steinbeck, I. D. White, H. N. Rojas, and R. W. Godby, Comput. Phys. Commun. **117**, 211 (1999).
[8] G. Onida, L. Reining, and A. Rubio, Rev. Mod. Phys. **74**, 601 (2002).
[9] M. Rohlfing, P. Krüger, and J. Pollmann, Phys. Rev. B **52**, 1905 (1995).
[10] M. Rohlfing and S. G. Louie, Phys. Rev. B **62**, 4927 (2000).
[11] L. X. Benedict, C. D. Spataru, and S. G. Louie, Phys. Rev. B **66**, 085116 (2002).
[12] X. Blase, C. Attaccalite, and V. Olevano, Phys. Rev. B **83**, 115103 (2011).
[13] C. Faber, C. Attaccalite, V. Olevano, E. Runge, and X. Blase, Phys. Rev. B **83**, 115123 (2011).

[14]L. Keldysh, Sov. Phys. JETP **20**, 1018 (1965).
[15]M. Wagner, Phys. Rev. B **44**, 6104 (1991).
[16]P. Danielewicz, Ann. Phys. **152**, 239 (1984).
[17]R. van Leeuwen, N. E. Dahlen, G. Stefanucci, C.-O. Almbladh, and U. von Barth, Lect. Notes Phys. **706**, 33 (2006).
[18]H. Haug and A. P. Jauho, *Quantum Kinetics in Transport and Optics of Semiconductors* (Springer-Verlag, Berlin, 1996).
[19]P. Myöhänen, A. Stan, G. Stefanucci, and R. van Leeuwen, Phys. Rev. B **80**, 115107 (2009).
[20]P. Myöhänen, A. Stan, G. Stefanucci, and R. van Leeuwen, Europhys. Lett. **84**, 67001 (2008).
[21]J. Rammer, *Quantum Field Theory of Non-Equilibrium States* (Cambridge University Press, Cambridge, 2007).
[22]G. Stefanucci and C.-O. Almbladh, Phys. Rev. B **69**, 195318 (2004).
[23]J. Rammer, Rev. Mod. Phys. **63**, 781 (1991).
[24]J. Rammer and H. Smith, Rev. Mod. Phys. **58**, 323 (1986).
[25]P. Danielewicz, Ann. Phys. **152**, 305 (1984).
[26]J. Schwinger, J. Math. Phys. **2**, 407 (1961).
[27]K. chao Chou, Z. bin Su, B. lin Hao, and L. Yu, Phys. Rep. **118**, 1 (1985).
[28]C. D. Spataru, L. X. Benedict, and S. G. Louie, Phys. Rev. B **69**, 205204 (2004).
[29]A. Stan, N. E. Dahlen, and R. van Leeuwen, Europhys. Lett. **76**, 298 (2006).
[30]N. E. Dahlen and R. van Leeuwen, Phys. Rev. Lett. **98**, 153004 (2007).
[31]A. Stan, N. E. Dahlen, and R. van Leeuwen, J. Chem. Phys. **130**, 114105 (2009).
[32]A. Stan, N. E. Dahlen, and R. van Leeuwen, J. Chem. Phys. **130**, 224101 (2009).
[33]K. S. Thygesen and A. Rubio, J. Chem. Phys. **126**, 091101 (2007).
[34]C. Rostgaard, K. W. Jacobsen, and K. S. Thygesen, Phys. Rev. B **81**, 085103 (2010).
[35]M. Puig von Friesen and C. Verdozzi, and C.-O. Almbladh, Phys. Rev. Lett. **103**, 176404 (2009).
[36]M. Puig von Friesen and C. Verdozzi, and C.-O. Almbladh, Phys. Rev. B **82**, 155108 (2010).
[37]U. Harbola and S. Mukamel, J. Chem. Phys. **124**, 044106 (2006).
[38]D. C. Langreth, Phys. Rev. B **1**, 471 (1970).
[39]P. Minnhagen, J. Phys. C **8**, 1535 (1975).
[40]W. G. Aulbur, C. Jönsson, and J. W. Wilkins, Solid State Phys. **54**, 1 (2000).
[41]P. Rinke, A. Qteish, J. Neugebauer, and M. Scheffler, Phys. Status Solidi B **4245**, 929 (2008).
[42]M. van Schilfgaarde, T. Kotani, and S. Faleev, Phys. Rev. Lett. **96**, 226402 (2006).
[43]H. J. deGroot, P. A. Bobbert, and W. van Haeringen, Phys. Rev. B **52**, 11000 (1995).
[44]U. von Barth and B. Holm, Phys. Rev. B **54**, 8411 (1996).
[45]E. L. Shirley, Phys. Rev. B **54**, 7758 (1996).
[46]P. Romaniello, S. Guyot, and L. Reining, J. Chem. Phys. **131**, 154111 (2009).
[47]B. Holm and U. von Barth, Phys. Rev. B **57**, 2108 (1998).
[48]B. Holm, Phys. Rev. Lett. **83**, 788 (1999).
[49]P. García-González and R. Godby, Phys. Rev. B **63**, 075112 (2001).
[50]G. Baym and L. P. Kadanoff, Phys. Rev. **124**, 287 (1961).
[51]K. Kaasbjerg and K. S. Thygesen, Phys. Rev. B **81**, 085102 (2010).
[52]A. Kutepov, S. Y. Savrasov, and G. Kotliar, Phys. Rev. B **80**, 041103(R) (2009).
[53]S. Faleev, M. van Schilfgaarde, and T. Kotani, Phys. Rev. Lett. **93**, 126406 (2004).
[54]M. Shishkin, M. Marsman, and G. Kresse, Phys. Rev. Lett. **99**, 246403 (2007).
[55]H. Jiang, R. Gomez-Abal, P. Rinke, and M. Scheffler, Phys. Rev. Lett. **102**, 126403 (2009).
[56]A. N. Chantis, M. van Schilfgaarde, and T. Kotani, Phys. Rev. B **76**, 165126 (2007).
[57]M. Giantomassi, M. Stankovski, R. Shaltaf, M. Grüning, F. Bruneval, P. Rinke, and G.-M. Rignanese, Phys. Status Solidi B **248**, 275 (2011).
[58]H. Ness, J. Phys. Condens. Matter **18**, 6307 (2006).
[59]L. K. Dash, H. Ness, and R. W. Godby, J. Chem. Phys. **132**, 104113 (2010).
[60]L. K. Dash, H. Ness, and R. W. Godby, Phys. Rev. B **84**, 085433 (2011).
[61]G. D. Mahan, *Many-Particle Physics* (Plenum, New York, 1990).
[62]C. Verdozzi, R. W. Godby, and S. Holloway, Phys. Rev. Lett. **74**, 2327 (1995).
[63]P. Minnhagen, J. Phys. C **7**, 3013 (1974).
[64]M. Stankovski *et al.* (unpublished).
[65]H. Ness, L. Dash, and R. W. Godby, Phys. Rev. B **82**, 085426 (2010).
[66]T. Kita, Prog. Theor. Phys. **123**, 581 (2010).
[67]V. Meden, C. Wöhler, J. Fricke, and K. Schönhammer, Phys. Rev. B **52**, 5624 (1995).
[68]P. Lipavský, V.Špička, and B. Velický, Phys. Rev. B **34**, 6933 (1986).
[69]A. L. Fetter and J. D. Walecka, *Quantum Theory of Many-Particle Systems* (McGraw-Hill, New York, 1971).
[70]T. Nagao, S. Yaginuma, T. Inaoka, and T. Sakurai, Phys. Rev. Lett. **97**, 116802 (2006).
[71]M. Strange, C. Rostgaard, H. Häkkinen, and K. S. Thygesen, Phys. Rev. B **83**, 115108 (2011).
[72]H. Mera, K. Kaasbjerg, Y. M. Niquet, and G. Stefanucci, Phys. Rev. B **81**, 035110 (2010).
[73]C. D. Spataru, M. S. Hybertsen, S. G. Louie, and A. J. Millis, Phys. Rev. B **79**, 155110 (2009).
[74]X. Wang, C. D. Spataru, M. S. Hybertsen, and A. J. Millis, Phys. Rev. B **77**, 045119 (2008).
[75]P. Darancet, A. Ferretti, D. Mayou, and V. Olevano, Phys. Rev. B **75**, 075102 (2007).
[76]The conventional equilibrium Green's formalism at finite temperature contains terms that are never considered at zero temperature, see p. 289 of Ref. 69.